DMD Fast Forward. Published on January 14, 2014 as doi:10.1124/dmd.113.054809
This article has not been copyedited and formatted. The final version may differ from this version.

Species difference in glucuronidation formation kinetics with a selective mTOR inhibitor

Loren M. Berry, Jingzhou Liu, Adria Colletti, Paul Krolikowski, Zhiyang Zhao, Yohannes Teffera

Departments of Pharmacokinetics and Drug Metabolism (L.M.B., J.L., A.C., Z.Z., Y.T) and Discovery Research (P.K.)

Amgen, Inc., Cambridge, MA 02142.

Running Title: Glucuronidation of an mTOR inhibitor

Corresponding Author: Yohannes Teffera
Amgen, Inc.
360 Binney St.
Cambridge, MA, 02142
loren.berry@amgen.com
Phone: 617-444-5240
Fax: 617-577-9609

Pages: 28

Tables: 3

Figures: 8

References: 19

Words: 251 (abstract)

482 (introduction)

1346 (discussion)

Non-standard abbreviations: CL, clearance; CLint, intrinsic clearance; IV, intravenous; LC-MS/MS, liquid chromatography tandem mass spectrometry; mTOR, mammalian target of rapamycin; PK, pharmacokinetics; UGT, UDP glucuronosyltransferase; NADPH, reduced nicotinamide adenine dinucleotide phosphate; AICc, Akaike information criterion corrected for small sample size

ABSTRACT

The mammalian target of rapamycin (mTOR) is a protein kinase that shows key involvement in age-related disease and promises to be target for treatment of cancer. In the present study, the elimination of potent ATP-competitive mTOR inhibitor 3-(6-amino-2-methylpyrimidin-4-yl)-N-(1H-pyrazol-3-yl)imidazo[1,2-b]pyridazin-2-amine (compound 1) is studied in bile duct cannulated rats, and the metabolism of compound 1 in liver microsomes is compared across species. Compound 1 was shown to undergo extensive N-glucuronidation in bile duct catheterized (BDC) rats. N-glucuronides were detected on positions N1 (M2) and N2 (M1) of the pyrazole moiety as well as on the primary amine (M3). All three N-glucuronide metabolites were detected in liver microsomes of the rat, dog and human, while primary amine glucuronidation was not detected in cynomolgus monkey. In addition N1 and N2-glucuronidation showed strong species selectivity *in vitro*, with rat, dog and human favoring N2-glucuronidation and monkey favoring N1-glucuronide formation. Formation of M1 in monkey liver microsomes also followed sigmoidal kinetics, singling out monkey as unique among the species with regard to compound 1 N-glucuronidation. In this respect, monkeys might not always be the best animal model for N-glucuronidation of UGT1A9 or UGT1A1 substrates in humans. The impact of N-glucuronidation of compound 1 could be more pronounced in higher species such as monkey and human leading to high clearance in these species. While compound 1 shows promise as a candidate for investigating the impact of pan-mTOR inhibition *in vivo*, opportunities may exist through medicinal chemistry effort to reduce metabolic liability with the goal of improving systemic exposure.

DMD Fast Forward. Published on January 14, 2014 as DOI: 10.1124/dmd.113.054809
This article has not been copyedited and formatted. The final version may differ from this version.

INTRODUCTION

The mammalian target of rapamycin (mTOR) is a serine/threonine protein kinase and a member of the phosphatidylinositol-3-OH kinase (PI3K) family (Lamming et al., 2013; Johnson et al., 2013). mTOR is active when associated with protein complexes that have differing functions and sensitivities to inhibition by rapamycin. mTOR complex 1 (mTORC1) is acutely sensitive to allosteric inhibitor rapamycin, while mTORC2 is acutely resistant, but ultimately, affected to some extent by chronic exposure to rapamycin. The biological functions of the mTOR complexes are to sense cellular availability of nutrients and other physiologically important signals such as amino acids, glucose, oxygen, WNT ligands, cAMP and insulin. As a result of these signals, mTORC1 activates translation and cell growth, while mTORC2 activates production of the cytoskeleton and phosphorylation of oncogenic AKT protein kinase. In particular, mTORC1 has been considered as a key modulator of several processes related to ageing and age-related disease. Indeed, inhibition of mTOR by rapamycin had been found to extend life span in a number of species, including mammals, with biological effects similar, but not necessarily identical, to those found following calorie/nutrient restriction (Lamming et al., 2013; Johnson et al., 2013; Fok et al., 2013). The mechanism(s) behind extended life span are still under investigation, however, a number of possible mechanisms have been proposed, including anticancer effects, reduced translation, increased autophagy, support of functional stem cells, modulation of immune response, reduced inflammation and improved mitochondrial function.

While use of mTOR inhibitors as treatments for extending life span or for other age-related diseases in humans is still theoretical, rapamycin and analogs everolimus

and temsirolimus have been approved for use in the treatment of a limited number of cancers (Benjamin et al., 2011). However, rapamycin and the analogs studied only incompletely inhibit mTORC1 phosphorylation, and selective inhibition of mTORC1 can increase AKT signaling by reducing negative feedback in the PI3K-mTORC2-AKT pathway. Therefore, second generation mTOR inhibitors, particularly ATP-competitive mTOR inhibitors that can more potently inhibit both mTORC1 and mTORC2, are being investigated for use in the oncology space, as well as to further elucidate the role of mTOR in ageing and disease (Benjamin et al., 2011; Schenone et al., 2011).

Previously, Peterson et al. (2012) described the discovery of a series of selective imidazopyridazine mTOR inhibitors. In particular, compound 1 (Figure 1) IC50 against mTOR was found to be 13 nM, with 58x selectivity over PI3Kα. Compound 1 exhibited moderate clearance following an intravenous dose to rats (2.3 L/h/kg), and approximately 100% bioavailability following oral dose. Solubility and bioavailability were greatly improved with compound 1 as compared to its imidazopyridine analog. Compound 1 shows promise as a tool for examining mTOR inhibition *in vivo*. However, little is known about the disposition of compound 1 across species. In the present study, the elimination of compound 1 is studied in bile duct cannulated rats and the metabolism of compound 1 in liver microsomes is compared across species.

DMD Fast Forward. Published on January 14, 2014 as DOI: 10.1124/dmd.113.054809
This article has not been copyedited and formatted. The final version may differ from this version.

MATERIALS AND METHODS

Materials

Compound 1 (>98% purity) was synthesized by the Medicinal Chemistry department at Amgen, Inc (Cambridge, MA) (Peterson et al., 2012). [^{14}C]- compound 1 (57.5 mci/mmol) was obtained from Moravek Biochemicals, Inc. (Brea, CA). All other compounds and reagents were obtained from commercial sources as appropriate. Liver microsomes isolated from male Sprague-Dawley rats (n>100), pooled male beagle dogs (n=5), pooled male cynomolgus monkey (n=10) and pooled male and female human (n=50) were purchased from BD Biosciences (San Jose, CA). Recombinant c-DNA expressed human UGT isoforms UGT1A1, UGT1A3, UGT1A4, UGT1A6, UGT1A7, UGT1A8, UGT1A9, UGT1A10, UGT2B4, UGT2B7, UGT2B15 and UGT2B17 were obtained from BD Biosciences, San Jose, CA.

Excretion studies in bile duct catheterized (BDC) rats

All animal procedures were conducted under protocols approved by the Amgen (Cambridge) Institutional Animal Care and Use Committee. Three male Sprague-Dawley rats were purchased from Charles River Laboratories (Wilmington, MA). The rats were housed in a humidity- and temperature-controlled environment subject to a 12 h:12 h light:dark cycle and had access to water and a standard laboratory diet *ad libitum*. Following a one week acclimation period, rats had Silastic catheters implanted in the bile duct and proximal duodenum using aseptic surgical techniques. The externalized catheters were protected with a Covance infusion harness (Instech Solomon, Plymouth Meeting, PA) and connected to permit recirculation of bile. The

DMD Fast Forward. Published on January 14, 2014 as DOI: 10.1124/dmd.113.054809
This article has not been copyedited and formatted. The final version may differ from this version.

BDC rats were placed in Nalge metabolism cages (Nalge Company, Rochester, NY) and given access to food and water *ad libitum*. The rats were fasted overnight prior to dosing; food was returned 2 h post-dose. On the second day post-surgery, the catheters were connected to a dual channel swivel (Instech Solomon, Plymouth Meeting, PA) for the collection of bile and the infusion of artificial bile (25 mM sodium taurocholate:150 mM NaCl:7 mM KCl, 2 mL/h) (Klaassen, 1974). Each BDC rat was administered a single dose of [^{14}C]- compound 1 (5 mg/kg, 100 µCi/kg PO). Bile, feces, and urine samples were collected at specified intervals through 48 h post-dose into pre-weighed bottles. The volume of bile and urine was determined gravimetrically, assuming a density of 1 g/mL.

Isolation of N-glucuronides from *in vitro* Incubations.

Ten milligrams of compound 1 (100 uM) was incubated with rat, dog, or monkey liver microsomes (2 mg protein/mL) in phosphate buffer (0.1 M, pH 7.4), with 10 mM MgCl2, 5 mM uridine-5'-diphosphoglucuronic acid (UDPGA), and 50 µg alamethicin/mg microsomal protein, for 4 h, at 37°C. The incubation mixture was extracted using an OASIS reverse phase cartridge (Waters Corporation, Milford, MA). The acetonitrile wash was evaporated and the sample was re-dissolved in HPLC mobile phase and separated using the system described under LC-MS analysis of BDC and *in vitro* samples. The HPLC eluate was split 1/20 with one part going to the MS and the rest to a Gilson FC 204 fraction collector (Gilson, Inc., Middleton, WI). The fraction containing the isolated glucuronide was dried, re-dissolved in HPLC solvent and subjected to further purification using a new HPLC column. The purity of the final product was determined by LC/MS (>90% for M1 and M2, >80% for M3).

Structural elucidation of N-glucuronide metabolites by NMR

All NMR spectra were acquired on a Bruker Avance II spectrometer system operating at a proton frequency of 600.13 MHz. The parent and isolated metabolites were dissolved in d6-DMSO and NMR data were collected in a 1.7 mm tubes using a Bruker 5 mm TCI cryo-probe. Proton and carbon assignments were made by using standard 1-D and 2-D pulse sequences. All NMR spectra were collected at a temperature of 26°C.

***In vitro* metabolism of compound 1**

For the identification of glucuronide metabolites in liver microsomes, radiolabeled compound 1 (10 µM, 28 mCi/mmol) was incubated with rat, dog, monkey, and human liver microsomes (1 mg protein /mL) in phosphate buffer (0.1 M, pH 7.4), with 10 mM $MgCl_2$ and 50 µg alamethicin/mg microsomal protein, for 1 h, at 37°C, with and without 5 mM uridine-5'-diphosphoglucuronic acid (UDPGA). The reaction mixtures were quenched with an equal volume of acetonitrile and centrifuged at 16,000 *g* for 5 min. The supernatant was diluted with an equal volume of 0.1% formic acid in water and analyzed by LC-MS/Radioflow following the method described under LC-MS analysis of BDC and *in vitro* samples.

Depletion of compound 1 in liver microsomes in the presence of NADPH was determined. Compound 1 (0.1 or 1 µM) was incubated with rat, dog, monkey or human liver microsomes (0.25 mg protein/mL) in phosphate buffer (0.1 M, pH 7.4), for 30 min (10 min for monkey liver microsomes), at 37°C, and in the presence of 1 mM NADPH,

DMD Fast Forward. Published on January 14, 2014 as DOI: 10.1124/dmd.113.054809
This article has not been copyedited and formatted. The final version may differ from this version.

and 10 mM $MgCl_2$. Samples were collected from the incubations at 0, 5, 10, 20, 30 and 40 minutes of incubation, and were quenched with an equal volume of acetonitrile and internal standard (a close analog of compound 1). Quenched samples were centrifuged at 4,000 *g* for 15 min and analyzed by LC-MS/MS. Intrinsic clearance (CLint) for compound 1 was calculated based on depletion half-life as described in Obach (1999).

To determine the kinetics of N-glucuronide formation in liver microsomes, compound 1 at 12 concentrations over a concentration range of 0.049 µM to 100 µM was incubated with rat, dog, monkey or human liver microsomes (0.5 mg protein/mL) in phosphate buffer (0.1 M, pH 7.4), for 30 min (10 min for monkey liver microsomes), at 37°C, and in the presence of 5 mM UDPGA, 10 mM $MgCl_2$ and 50 µg alamethicin/mg microsomal protein. The reaction mixtures were quenched with an equal volume of acetonitrile and centrifuged at 4,000 *g* for 15 min. Supernatants were transferred to new vessels and dried to completion under a stream of nitrogen. Dried samples were reconstituted in an equal volume of 10% acetonitrile, 0.1% formic acid, 90% H_2O containing 1 µM internal standard (a close analog of compound 1). N-glucuronide metabolites were isolated and purified by LC-fraction collection from bulk incubations with liver microsomes to serve as analytical standards. Analytical standards were prepared in liver microsomes matrix with purified N-glucuronides at a concentration range of 0.02 µM to 25 µM. Standards were processed in the same fashion as described above for samples. Samples and standards were analyzed by LC-MS/MS.

For the reaction phenotyping of compound 1 metabolism in human UGT isoforms, compound 1 was incubated at final concentrations of 0.1 µM, 1 µM or 10 µM with c-DNA expressed human UGT1A1, UGT1A3, UGT1A4, UGT1A6, UGT1A7, UGT1A8, UGT1A9, UGT1A10, UGT2B4, UGT2B7, UGT2B15 and UGT2B17. UGT

isoforms and compounds were incubated at 0.25 mgs of enzyme/mL, in the presence of 5 mM UDPGA, 10 mM $MgCl_2$, 50 µg alamethicin/mg microsomal protein, at 37°C, and for 2 h. The reaction mixtures were quenched with an equal volume of acetonitrile and centrifuged at 14,000 rpm for 5 min. The supernatant was diluted with an equal volume of 0.1% formic acid in water and analyzed by LC-MS/MS.

LC-MS analysis of BDC and *in vitro* samples

For metabolite identification in radiolabeled or non-radiolabeled samples from BDC and *in vitro* experiments, the LC-MS/MS system consisted of a Shimadzu LC-20AD HPLC system (Shimadzu USA, Palo Alto, CA), a Thermo LTQ Orbi-Trap mass spectrometer (ThermoElectron Corp., San Jose, CA), and a Radiomatic 625 Flow Scintillation Analyzer (PerkinElmer Life and Analytical Sciences, Downers Grove, IL). The LTQ-Orbitrap was equipped with an API2 source and Xcalibur version 2.0 software (Thermo Electron Corp., San Jose, CA). All mass spectra were acquired in the high resolution mode using 30,000 resolving power. Exact mass measurement was accomplished using external calibration. Electrospray ionization with positive ion detection was used. The source temperature was set at 250°C, and the ion spray voltage was held at 4.5 kV. Pooled rat bile (0-48 hr, 5 µL), pooled rat urine (0-48 hr, 100 µL), or *in vitro* samples were loaded onto a YMC-AQ C18-A column (Torrance, CA) 4.6 x 250 mm, 5 µm particle size, 120 Å pore size). The metabolites were separated using a gradient solvent system consisting of two components, solvent A (0.1% formic acid in water) and solvent B (0.1% formic acid in acetonitrile). The percentage of solvent B was held at 5% for 3 minutes, then was increased in a linear fashion from 5% to 30% B over 37 minutes, and from 30% to 95% B in the next 10 minutes. The flow

rate was set at 1.0 mL/min and the column eluate was split 1:20, with one part channeled to the ion source and the rest to the flow scintillation analyzer (waste for non-radiolabeled samples or fraction collector for isolation). The MS/MS spectra were recorded by collision-induced dissociation (CID) of $[M+H]^+$ species.

Samples from compound 1 depletion and N-glucuronide formation kinetics studies were analyzed by multiple reaction monitoring on an LC-MS/MS system consisting of dual Shimadzu LC-10AD HPLC pumps and a DGU-14A degasser (Shimadzu, Columbia, MD), a CTC PAL autoinjector (Leap Technologies, Carrboro, NC), and an API4000 MS system, equipped with an electrospray ion source and operated by the Analyst software package (Applied Biosystems, Foster City, CA). The source temperature was set to 400°C, and the ion spray voltage was set to 4.5kV. Chromatography was conducted on a YMC ODS-AQ (50 x 4.6mm, 5µm) analytical column with a 0.5 µm PEEK guard filter, using the mobile phase solvents A and B described above at a flow rate of 0.7 mL/min. The percentage of solvent B was increased in a linear fashion from 2% to 18% over 7 minutes, then from 18% to 90% in the next 0.5 minutes and held at 90% for the next 2 minutes, when it was then returned to 2%. The LC eluent was diverted from the ion source to waste for the first 3 minutes of each sample run. Compound 1 (*m/z* 308 → 250), N-glucuronides (*m/z* 484 → 308), and internal standard (*m/z* 322 → 264) were detected in positive ion mode.

Modeling of N-glucuronide metabolite formation kinetics

In order to determine which kinetic model(s) to use, Eadie-Hofstee plots were created using the reaction velocity data from each metabolite in liver microsomes of each species. Based on the appearance of the data in this plot, one of the following

models (below) was used to describe the data. Kinetics parameters were fit by non-linear regression, and metabolite formation was simulated, using GraphPad Prism v6.02 (GraphPad Software Inc., San Diego, CA). In addition, the choice of model was supported by comparison against possible competing models using the model comparison feature in Graphpad Prism. Preferred models were confirmed based on difference in AICc. Metabolite formation with an apparently linear Eadie-Hofstee plot were described by a single enzyme model assuming standard Michaelis-Menten kinetics (one-site),

$$v = \frac{V_{\max} * C}{K_m + C} \qquad \text{Eq. 1}$$

where v is the reaction velocity, V_{max} is the maximum reaction velocity, K_m is the concentration required to achieve 50% of the maximum reaction velocity, and C is the concentration of compound 1 in the incubation. Metabolite formation where the Eadie-Hofstee plot appeared bi-phasic were described by a two enzyme model (two-site),

$$v = \frac{V_{\max,h} * C}{K_{m,h} + C} + \frac{V_{\max,l} * C}{K_{m,l} + C} \qquad \text{Eq. 2}$$

where the subscripts h and l indicate V_{max} and K_m parameters for the high and low affinity enzymes, respectively. Metabolite formation where the Eadie-Hofstee plot

appeared biphasic with an apparent decrease in v with decreasing v/[S] values were described by a single enzyme model with substrate inhibition (one-site SI),

$$v = \frac{V_{\max} * C}{K_m + C * (1 + \frac{C}{K_{i,si}})} \quad \text{Eq. 3}$$

Where $K_{i,si}$ is the inhibition constant for the substrate inhibition. Metabolite formation where the Eadie-Hofstee plot appeared triphasic with an apparent decrease in v with decreasing v/[S] values were described by a two enzyme model with substrate inhibition (two-site SI),

$$v = \frac{V_{\max,h} * C}{K_{m,h} + C} + \frac{V_{\max,l} * C}{K_{m,l} + C * (1 + \frac{C}{K_{i,si}})} \quad \text{Eq. 4}$$

where the substrate inhibition is considered to occur against the low affinity enzyme. Finally, non-Michaelis-Menten kinetics displaying cooperativity was described by,

$$v = \frac{V_{\max} * C^n}{K_m{}^n + C^n} \quad \text{Eq. 5}$$

where *n* is the Hill coefficient.

RESULTS

Metabolism and excretion of [^{14}C]-compound 1 in BDC rats

Following oral administration of [^{14}C]-compound 1 approximately 52% of the radioactivity was recovered in bile, with another 10% recovered in urine, and 14% recovered in feces after 48 hours. Radiochromatograms of bile and urine are shown in Figure 2. Amount of radioactivity in bile and urine attributable to compound 1 was minimal (<5% of dose). Several major metabolite peaks were visible in the bile and/or urine, labeled M1 – M4. M1 – M3 were detected in both urine and bile, and were found to have an accurate mass (*m/z*) of 484.169 amu, corresponding to direct glucuronidation of compound 1 at three distinct locations of the parent molecule. The product ion spectra (Figure 3) of the glucuronides were similar and produced the parent (*m/z* 308.138) and the fragments of the parent (within <4 ppm). Therefore, the exact positions of the glucuronides could not be elucidated using the product ion data. M4 was detected in bile but not urine, and was found to have an accurate mass (*m/z*) of 500.164 amu, corresponding to oxidation and glucuronidation of the parent. Subsequent analysis revealed that treatment of bile samples with glucuronidase caused the degradation of M4 to M5, found to have an accurate mass (*m/z*) of 324.132 amu, and corresponding to hydroxylation of compound 1. M4 was then concluded to be an –O-glurcuronide of compound 1. M1 – M3 were stable in the presence of glucuronidase.

Structural elucidation of N-glucuronide metabolites by NMR

In order to elucidate the structures of metabolites formed by direct glucuronidation of compound 1, M1 – M3 were isolated and purified by fraction

collection. The NMR studies of the isolated glucuronide metabolites were conducted by dissolving the metabolites (~100 µg) in 50 µL of DMSO-d6 and placing the samples in a 1.7 mm tubes for data collection. The proton and carbon assignments were obtained from the 1D (1H) and 2D (g-DQCOSY, g-HSQCdept, gradient-heteronuclear multiple bond correlation (g-HMBC), rotating-frame Overhauser effect spectroscopy (ROESY)) spectra collected on the samples (Table 1). The NMR spectra are consistent with the structures shown in Figure 1. Glucuronide 1 (M1) was attached to N2 of the pyrazole ring and demonstrated by connections in the g-HMBC spectrum between H1□ and C3. In the ROESY spectrum of glururonide 1, a cross-peak was observed between the anomeric proton H1□ and the secondary amine labeled 6. The attachment of glucuronide 2 (M2) was verified by g-HMBC connections between H1□ and C5. The ROESY spectrum of glucuronide 2 presents cross-peaks between glucuronide protons H1□ and H2□ to H5. The attachment of a glucuronide at position 1 or 2 of the pyrazole moiety induced a shift in the double bonds of that ring in order to accommodate the substitution. In glucuronide 1, a double bond exists between N1 and C5. This double bond de-shields carbon 5 and causes ~10 ppm shift of the carbon resonance. This effect was also observed in glucuronide 2 for C3. These chemical shift changes were used to track substitutions of many synthetic analogs at both positions of the pyrazole ring. For glucuronide 3 (M3), there were ROESY cross-peaks observed between H21 and an anomeric proton at 5.30 ppm and two other glucuronide methine protons at 3.91 and 3.51 ppm. Based on the results of the LC-MS and NMR data the scheme for the metabolism of compound 1 in rats was proposed as shown in Figure 1.

DMD Fast Forward. Published on January 14, 2014 as DOI: 10.1124/dmd.113.054809
This article has not been copyedited and formatted. The final version may differ from this version.

Metabolism of compound 1 in liver microsomes

Experiments were conducted using rat, dog, monkey and human liver microsomes to investigate the similarity of metabolism of compound 1 across species. Preliminary experiments in the presence of UDPGA revealed that all three N-glucuronides observed in BDC rats were formed from rat liver microsomes with similar relative abundances, M1 > M2 > M3 (Figure 4). This suggests that liver microsomes are a suitable enzyme source for investigating N-glucuronide formation from compound 1 *in vitro*. Looking across species, M1 and M2 were formed by liver microsomes from all species tested, albeit to different extents. Formation of M3 was detected in rat, dog and human, but not monkey, liver microsomes. No other glucuronides were detected with liver microsomes *in vitro*. At a concentration of 10 μM, formation of M1 was substantially greater than formation of M2 or M3 in dog and human liver microsomes. However, M2 was the major metabolite in monkey liver microsomes. Experiments with liver microsomes fortified with NADPH indicated that compound 1 undergoes rapid oxidative metabolism in dog and monkey liver microsomes, while that in rat and human liver microsomes occurs more slowly (Table 2).

Metabolite formation experiments were conducted in order to further characterize the apparent species dependence in N-glucuronide formation. Concentration dependence in formation kinetics was described by a number of different kinetic models, depending on the appearance of Eadie-Hofstee plots. M1 formation was most accurately described by two-enzyme kinetic models in rat, dog and human liver microsomes, indicating the M1 is most likely primarily formed by two major UGT isoforms, within each of these species (Figure 5). In dog, a substrate inhibition effect

was also required to describe the decreasing reaction velocity at the highest compound 1 concentrations tested. The model fit best when substrate inhibition was applied to the low affinity binding site, rather than the high affinity binding site or both binding sites simultaneously. Formation of M1 in monkey liver microsomes displayed atypical kinetics and was described by a sigmoid function incorporating a Hill slope of 1.54 ± 0.03, indicating positive cooperativity. V_{max} values for M1 formation showed considerable variation across the species tested (Table 3). M2 formation was most accurately described by single-enzyme kinetic models. Models for M2 formation in dog, monkey and human liver microsomes fit best when a substrate inhibition effect was included. Substrate inhibition was not required to fit the formation of M2 in rat liver microsomes. Values for V_{max} and K_m showed a 10-fold or greater variation across species. One site kinetic models were also fit to the formation of M3. In some cases (rat and dog liver microsomes) required a substrate inhibition effect. M3 was not detected in incubations with monkey liver microsomes.

Formation of N-glucuronides in human UGTs

M1 was formed principally by UGT1A1 and UGT1A9 (Figure 8). M1 was also formed to a minor extent in UGT1A3, UGT1A7 and UGT1A8. Both M2 and M3 were principally formed by UGT1A9. M2 was formed to a minor extent in UGT1A1 and UGT1A3. M3 was formed to a minor extent in UGT1A1, UGT1A3, UGT1A4 and UGT1A8. No glucuronides were detected in incubations with UGT1A6, UGT1A10, UGT2B4, UGT2B7, UGT2B15 and UGT2B17. In addition, no other glucuronides (besides M1 – M3) were observed in incubations with isolated human UGTs.

Interestingly, some concentration dependence was observed in the metabolic profile of compound 1 when incubated with UGT1A9. At low concentrations (0.1 µM), M2 was the main metabolite formed from UGT1A9 while at high concentrations (10 µM), M1 was the major metabolite.

DISCUSSION

The mTOR inhibitor compound 1 was extensively glucuronidated in rats. Substantial quantities of N-glucuronides, but minimal parent (<5% of dose), were found in both urine and bile of BDC rats dosed orally with compound 1. Although compound 1 contains several possible locations for direct N-glucuronidation, glucuronidation was detected only on N1 and N2 of the pyrazole moiety as well as on the primary amine (N23). No glucuronidation was detected on the secondary amine (N6) or tertiary amines (N8, N10, N11, N17 or N19). In addition, other glucuronides species such as carbamoyl glucuronides (Schaefer, 2006) were not detected in rat bile or urine. However, it cannot be ruled out that such glucuronides exist, perhaps in quantities that are below the detection limits of radiochemical or LC-MS detection. Interestingly, the relative abundance of the three N-glucuronides were similar between urine and feces, with M1 being the major metabolite in urine and bile, and M2 and M3 formed to a smaller, though significant, extent. Since minimal (≤10% of parent) N-glucuronides were detected in rat plasma following an oral dose of compound 1 (unpublished data), it is possible that the N-glucuronides found in urine were formed by UGT enzymes in the kidney, perhaps by the same enzymes responsible for their formation in the liver. However, given the wide tissue expression of UGT mRNA and activity in rats, their formation by other extrahepatic tissues cannot be ruled out at this time (Shelby et al., 2003; Shiratani et al., 2008). Since the total quantity of dose excreted in urine was minor relative to that in bile (10% versus 52%, respectively), and oxidative metabolism was also a minor pathway, further detailed investigation of compound 1 metabolism was focused on N-glucuronide formation in liver microsomes, particularly, given available

documentation that species differences in N-glucuronidation of aromatic N-heterocycles can be highly compound dependent (Kaivosaari et al., 2011).

When incubated in rat liver microsomes in the presence of UDPGA, Compound 1 formed the same three glucuronides found *in vivo* to similar proportions, M1>M2>M3 (Figure 4). This helped to established confidence that liver microsomes were a reasonable enzyme source for investigating N-glucuronidation of compound 1. Qualitative and quantitative species differences were found in the metabolism of compound 1 by liver microsomes, as were there some similarities. Firstly, all three N-glucuronides were detected in liver microsomes from dogs and humans. However, while M1 and M2 were detected in liver microsomes from monkeys, M3 was not detected. No other N-glucuronides were detected in liver microsomes from all species tested.

Secondly, M3 was consistently the relatively minor metabolite of the three, across three of the species tested (rat, dog and human), or undetected in monkey (Figure 4). However, at low concentrations (10 μM or less), M1 was the major metabolite formed in rat, dog and human liver microsomes, while M2 was the major metabolite formed in monkey liver microsomes. This species selectivity found in monkeys is unique when compared to other recent examples of triazole and pyrazole N-glucuronidation. In the case of FYX-051, the ratios of N1- to N2-glucuronide formation *in vivo* were quite similar in dogs, monkey and humans (Nakazawa et al., 2006). In the case of JNJ-10198409, the N1-glucuronide was prominently formed in both monkey and human liver microsomes, while the N2-glucuronide was not detected in either species (Yan et al., 2006). The reasons for the unique species selectivity with compound 1 are

not currently known. Compound 1 was found to be metabolized primarily by UGT1A9 and UGT1A1 in humans *in vitro*. UGT1A1 is more or less conserved across species given its important role in bilirubin metabolism (Bosma et al., 1994; King et al., 1996). However, species differences have been reported in activity of UGT1A9. Dog and rat apparently lack meaningful propofol glucuronidation activity and *UGT1A9* is a pseudogene in rats (Soars et al., 2001; Shiratani et al., 2008). In addition, monkey and human UGT1A9 orthologs were found to be 93% homologous, and structurally and functionally similar (Albert et al., 1999). Such findings have supported the belief that rats and dogs are not predictive of glucuronidation by UGT1A9 substrates, and that monkeys might be a better model for this purpose. However, the present findings with compound 1 suggest that this might not always be the case. Given this unique species selectivity, compound 1 might be a useful probe to investigate such species differences in UGT functionality.

Thirdly, detailed kinetic analysis of N-glucuronide formation can shed further light on the apparent species differences and similarities. M1 formation was biphasic in rat, dog and human liver microsomes indicating that two enzymes, one high affinity and one low affinity, are responsible for M1 formation in these species *in vitro* (Figure 5). In humans this conclusion is supported by reaction phenotyping experiments, which confirmed that UGT1A1 and UGT1A9 predominantly formed M1 *in vitro*. If UGT1A1 is assumed to be one of the UGTs responsible for M1 formation in rats and dogs, another UGT, besides UGT1A9, might be implied as the second enzyme, given UGT1A9 activity was found to be lacking in rats and dogs. Since other human UGTs were found to have minor activity in compound 1 N-glucuronidation, perhaps rat or dog orthologs of these UGTs are more important in these species. In monkey liver microsomes, M1 was

formed in a fashion consistent with single enzyme sigmoidal kinetics, requiring a Hill slope, indicative of positive cooperativity or auto-activation. This type of kinetics was unique among the species and compared to M2 formation in monkey liver microsomes. It is not currently known whether monkey UGT1A1 or UGT1A9 contributed to this kinetics, or what the specific nature of the mechanism behind the kinetics might be. Nevertheless this observation supports the uniqueness of monkeys among species in the N-glucuronidation of compound 1. Aside from some clear capacity differences across species, formation of M2 and M3 were more similar across species, following single enzyme kinetics. The finding in human liver microsomes was supported by additional reaction phenotyping experiments, where M2 and M3 were formed principally by a single UGT, UGT1A9. Generally, capacity for compound 1 N-glucuronidation was much higher in human and monkey liver microsomes than in rat or dog liver microsomes, but the metabolic profiles in rats and dogs were qualitatively more similar to that in humans *in vitro*.

Reaction phenotyping experiments with compound 1 also have potential clinical relevance. Since compound 1 N-glucuronidation occurred predominantly by UGT1A1 and UGT1A9, care must be taken to avoid potential drug interactions with potent inhibitors of these enzymes. However, having more than one UGT responsible, in addition to any oxidation metabolism, may help limit effects of inhibition of any single UGT. In addition, since UGT1A1 is highly expressed in the human intestine (Rowland et al., 2013), inhibition of UGT1A1, or known polymorphisms, could impact the bioavailability of compound 1, if bioavailability is limited by metabolism by UGT1A1 in the gut. Further *in vitro* and physiological modeling studies might be warranted to clarify the potential impact of UGT inhibition or polymorphisms.

In summary, compound 1 was shown to undergo extensive N-glucuronidation in BDC rats. N-glucuronides were detected on positions N1 (M2) and N2 (M1) of the pyrazole moiety as well as on the primary amine (M3). All three N-glucuronide metabolites were detected in liver microsomes of the rat, dog and human, while primary amine glucuronidation (M3) was not detected in monkey. In addition N1- and N2-glucuronidation showed strong species selectivity *in vitro*, with rats, dogs and humans favoring N2-glucuronidation and monkeys favoring N1-glucuronide formation. Formation of M1 (N2-glucuronidation) in monkey liver microsomes also followed sigmoidal kinetics, singling out monkey as unique among the species as far as compound 1 N-glucuronidation. In this respect, monkey might not always be the best animal model for N-glucuronidation of UGT1A9 or UGT1A1 substrates in humans. Impact of N-glucuronidation could be more pronounced in higher species such as monkey and human, leading to high clearance in these species. While compound 1 shows promise as a candidate for investigating the impact of pan-mTOR inhibition *in vivo*, opportunities may exists through medicinal chemistry effort to potentially reduce metabolic liability with the goal of improving systemic exposure.

DMD Fast Forward. Published on January 14, 2014 as DOI: 10.1124/dmd.113.054809
This article has not been copyedited and formatted. The final version may differ from this version.

Acknowledgements

We thank Meghan Canfield and John Roberts for conducting the *in vivo* procedures.

Authorship Contributions

Participated in research design: Berry, Colletti, Teffera and Zhao

Conducted experiments: Berry, Colletti, Krolikowski, and Liu

Performed data analysis: Berry, Colletti, Liu, Krolikowski, and Teffera

Wrote or contributed to the writing of the manuscript: Berry, Krolikowski, Teffera, and Zhao

REFERENCES

Benjamin D, Colombi M, Moroni C, and Hall MN (2011) Rapamycin passes the torch: a new generation of mTOR inhibitors. *Nat Rev Drug Discov* **10**:868-880.

Bosma PJ, Seppen J, Goldhoorn B, Bakker C, Oude Elferink RP, Chowdhury JR, Chowdhury NR, and Jansen PL (1994) Bilirubin UDP-glucuronosyltransferase 1 is the only relevant bilirubin glucuronidating isoform in man. *J Biol Chem* **269**:17960-17964.

Fok WC, Zhang Y, Salmon AB, Bhattacharya A, Gunda R, Jones D, Ward W, Fisher K, Richardson A, and Pérez VI (2013) Short-term treatment with rapamycin and dietary restriction have overlapping and distinctive effects in young mice. *J Gerontol A Biol Sci Med Sci* **68**:108-116.

Johnson SC, Rabinovitch PS, and Kaeberlein M (2013) mTOR is a key modulator of ageing and age-related disease. *Nature* **493**:338-345.

Kaivosaari S, Finel M, and Koskinen M (2011) N-glucuronidation of drugs and other xenobiotics by human and animal UDP-glucuronosyltransferases. *Xenobiotica* **41**:652-669.

King CD, Green MD, Rios GR, Coffman BL, Owens IS, Bishop WP, and Tephly TR (1996) The glucuronidation of exogenous and endogenous compounds by stably expressed rat and human UDP-glucuronosyltransferase 1.1. *Arch Biochem Biophys* **332**(1):92-100.

Klaassen CD (1974) Bile flow and composition during bile acid depletion and administration. *Can J Physiol Pharmacol* **52**:334-348.

Lamming DW, Ye L, Sabatini DM, and Baur JA (2013) Rapalogs and mTOR inhibitors as anti-aging therapeutics. *J Clin Invest* **123**:980-989.

Nakazawa T, Miyata K, Omura K, Iwanaga T, and Nagata O (2006) Metabolic profile of FYX-051 (4-(5-pyridin-4-yl-1h-[1,2,4]triazol-3-yl)pyridine-2-carbonitrile) in the rat, dog, monkey, and human: identification of N-glucuronides and N-glucosides. *Drug Metab Dispos* **34**:1880-1886.

Obach RS (1999) Prediction of human clearance of twenty-nine drugs from hepatic microsomal intrinsic clearance data: An examination of in vitro half-life approach and nonspecific binding to microsomes. *Drug Metab Dispos* **27**:1350-1359.

Peterson EA, Boezio AA, Andrews PS, Boezio CM, Bush TL, Cheng AC, Choquette D, Coats JR, Colletti AE, Copeland KW, DuPont M, Graceffa R, Grubinska B, Kim JL, Lewis RT, Liu J, Mullady EL, Potashman MH, Romero K, Shaffer PL, Stanton MK, Stellwagen JC, Teffera Y, Yi S, Cai T, and La DS (2012) Discovery and optimization of potent and selective imidazopyridine and imidazopyridazine mTOR inhibitors. *Bioorg Med Chem Lett* **22**:4967-4974.

Rowland A, Miners JO, and Mackenzie PI (2013) The UDP-Glucuronosyltransferases: their role in drug metabolism and detoxification. Int J Biochem Cell Biol. Mar 7 (Epub ahead of print).

Schaefer WH (2006) Reaction of primary and secondary amines to form carbamic acid glucuronides. Curr Drug Metab 7:873–881.

Schenone S, Brullo C, Musumeci F, Radi M, and Botta M (2011) ATP-competitive inhibitors of mTOR: an update. *Curr Med Chem* **18**:2995-3014.

Shelby MK, Cherrington NJ, Vansell NR, and Klaassen CD (2003) Tissue mRNA expression of the rat UDP-glucuronosyltransferase gene family. *Drug Metab Dispos* **31**:326-333.

Shiratani H, Katoh M, Nakajima M, Yokoi T. (2008) Species differences in UDP-glucuronosyltransferase activities in mice and rats. *Drug Metab Dispos* **36**:1745-1752.

Soars MG, Riley RJ, and Burchell B (2001a) Evaluation of the marmoset as a model species for drug glucuronidation. *Xenobiotica* **31**:849-860.

Soars MG, Riley RJ, Findlay KA, Coffey MJ, and Burchell B (2001b) Evidence for significant differences in microsomal drug glucuronidation by canine and human liver and kidney. *Drug Metab Dispos* **29**:121-126.

Yan Z, Caldwell GW, Gauthier D, Leo GC, Mei J, Ho CY, Jones WJ, Masucci JA, Tuman RW, Galemmo RA Jr, and Johnson DL (2006) N-glucuronidation of the platelet-derived growth factor receptor tyrosine kinase inhibitor 6,7-(dimethoxy-2,4-dihydroindeno[1,2-C]pyrazol-3-yl)-(3-fluoro-phenyl)-amine by human UDP-glucuronosyltransferases. *Drug Metab Dispos* **34**:748-755.

Legends for Figures

Figure 1. Biotransformation of compound 1 *in vivo* and *in vitro.*

Figure 2. Radiochromatographic profile of [^{14}C]-compound 1 and metabolites in bile, bile treated with glucuronidase, and urine from bile-duct cannulated male rats following a 5 mg/kg oral dose of [^{14}C]-compound 1.

Figure 3. Product ion mass spectra of a) MH^+ ion of compound 1 (*m/z* 308), and b) MH^+ ion of glucuronide (*m/z* 484).

Figure 4. Radiochromatograms of [^{14}C]-compound 1 and metabolites in rat, dog, monkey, and human liver microsomes fortified with UDPGA.

Figure 5. Formation of M1 from compound 1 in incubations of rat (A), dog (B), monkey (C) and human (D) liver microsomes fortified with UDPGA. Inserts in each panel are the Eadie-Hofstee diagrams of the same data displayed in the main reaction velocity plots.

Figure 6. Formation of M2 from compound 1 in incubations of rat (A), dog (B), monkey (C) and human (D) liver microsomes fortified with UDPGA. Inserts in each panel are the Eadie-Hofstee diagrams of the same data displayed in the main reaction velocity plots.

Figure 7. Formation of M3 from compound 1 in incubations of rat (A), dog (B), and human (C) liver microsomes fortified with UDPGA. Inserts in each panel are the Eadie-Hofstee diagrams of the same data displayed in the main reaction velocity plots.

Figure 8. Reconstructed ion chromatogram (*m/z* 308 and 484) of compound 1 and N-glucuronide metabolites formed by UGT1A1 (A) and UGT1A9 (B) at 0.1 µM, 1 µM, and 10 µM.

DMD Fast Forward. Published on January 14, 2014 as DOI: 10.1124/dmd.113.054809
This article has not been copyedited and formatted. The final version may differ from this version.

TABLES

Table 1: Carbon and proton chemical shift assignments for compound 1, and N-glucuronides 1 (M1) and 2 (M2) in DMSO-*d6*.

Position	Group	Parent		N-glucuronide 1		N-glucuronide 2	
		δ (^{13}C) ppm[a]	δ (^{1}H) ppm[b]	δ (^{13}C) ppm[a]	δ (^{1}H) ppm[b]	δ (^{13}C) ppm[a]	δ (^{1}H) ppm[b]
1	NH	-	12.16	-	-	-	-
3	C	148.9	-	140.0	-	149.0	-
4	CH	94.1	6.83	93.5	6.71	96.1	6.94
5	CH	128.4	7.64	138.8	7.48	130.6	7.81
6	NH	-	11.10	-	11.24	-	11.13
7	C	-	-	-	-	-	-
9	C	139.2	-	139.0	-	139.1	-
12	CH	141.2	8.57	141.9	8.64	141.6	8.59
13	CH	116.8	7.31	117.4	7.36	117.3	7.33
14	CH	121.5	8.02	122.4	8.10	122.1	8.05
15	C	105.1	-	105.8	-	105.4	-
16	C	152.8	-	152.4	-	153.1	-
18	C	165.2	-	165.7	-	165.3	-
20	C	164.1	-	164.1	-	164.0	-
21	CH	93.5	7.66	93.8	7.69	93.8	7.67
22	CH_3	25.5	2.45	25.9	2.50	26.1	2.46
23	NH_2	-	6.96	-	7.06	-	6.97
1□	CH	-	-	84.1	5.17	88.5	5.22
2□	CH	-	-	70.9	3.96	70.8	3.79
3□	CH	-	-	77.5	3.36	76.4	3.40
4□	CH	-	-	71.6	3.25	71.0	3.47
5□	CH	-	-	75.9	3.48	72.3	3.79
6□	C=O	-	-	171.3	-	167.6	-

[a] Carbon chemical shifts are measured relative to the DMSO-d6 signal at 39.51 ppm.

[b] Proton chemical shifts are measured relative to the DMSO-d6 signal at 2.50 ppm□.

DMD Fast Forward. Published on January 14, 2014 as DOI: 10.1124/dmd.113.054809
This article has not been copyedited and formatted. The final version may differ from this version.

Table 2. Depletion of compound 1 in liver microsomes fortified with NADPH

	CL_{int} (µL/(min*mg))			
Conc. (µM)	Rat	Dog	monkey	Human
0.1	86	307	554	69
1	26	97	209	18

DMD Fast Forward. Published on January 14, 2014 as DOI: 10.1124/dmd.113.054809
This article has not been copyedited and formatted. The final version may differ from this version.

Table 3: Best fit for the model parameters describing the formation of N-glucuronides from compound 1 in rat, dog, monkey and human liver microsomes fortified with UDPGA.

N-glucuronide/model parameter		rat	dog	monkey	human
M1	model	two-site	two-site SI	sigmoid	two-site
	$v_{max,h}$ (pmol/(min*mg))	1.34 ± 0.25	0.362 ± 0.107	217 ± 5	33.5 ± 11.3
	$k_{m,h}$ (µM)	0.787 ± 0.248	1.42 ± 0.40	26.2 ± 0.9	3.55 ± 0.88
	$v_{max,l}$ (pmol/(min*mg))	2.60 ± 0.20	1.63 ± 3.20	NA	44.6 ± 9.5
	$k_{m,l}$ (µM)	19.0 ± 5.5	65.2 ± 178.3	NA	22.7 ± 9.6
	$K_{i,si}$ (µM)	NA	15.8 ± 44.8	NA	NA
	n	NA	NA	1.54 ± 0.03	NA
M2	model	one-site	one-site SI	one-site SI	one-site SI
	v_{max} (pmol/(min*mg))	1.82 ± 0.04	0.0965 ± 0.0171	213 ± 4	14.5 ± 0.5
	k_m (µM)	2.42 ± 0.20	15.0 ± 4.7	7.76 ± 0.31	25.4 ± 1.4
	$K_{i,si}$ (µM)	NA	191 ± 111	98.9 ± 5.3	86.4 ± 6.4
M3	model	one-site SI	one-site SI	NA	one-site
	v_{max} (pmol/(min*mg))	0.0696 ± 0.0021	0.323 ± 0.023	NA	0.258 ± 0.008
	k_m (µM)	1.14 ± 0.11	10.6 ± 1.5	NA	15.0 ± 1.4
	$K_{i,si}$ (µM)	375 ± 93	271 ± 86	NA	NA

NA indicates not applicable

DMD Fast Forward. Published on January 14, 2014 as DOI: 10.1124/dmd.113.054809
This article has not been copyedited and formatted. The final version may differ from this version.

Figure 1

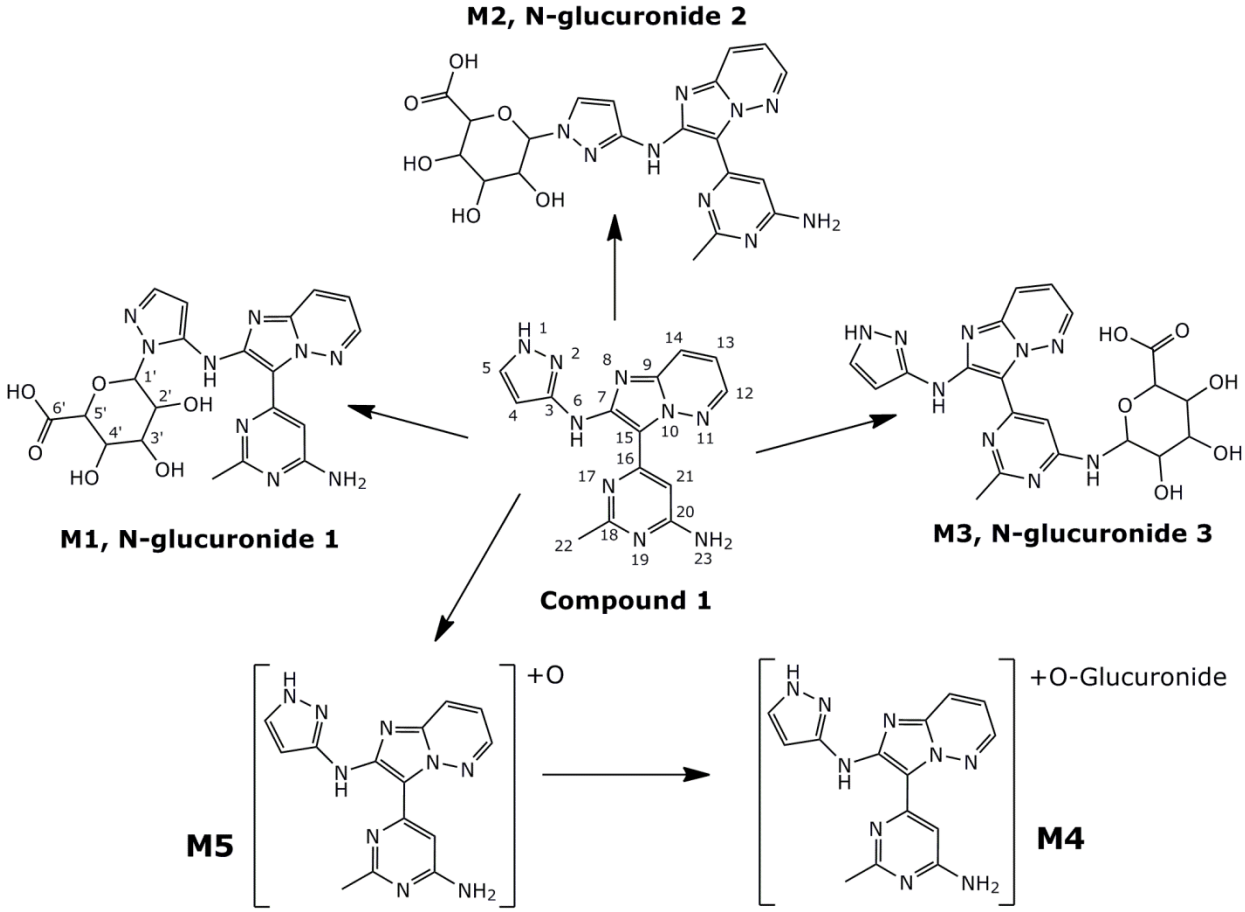

DMD Fast Forward. Published on January 14, 2014 as DOI: 10.1124/dmd.113.054809
This article has not been copyedited and formatted. The final version may differ from this version.

Figure 2

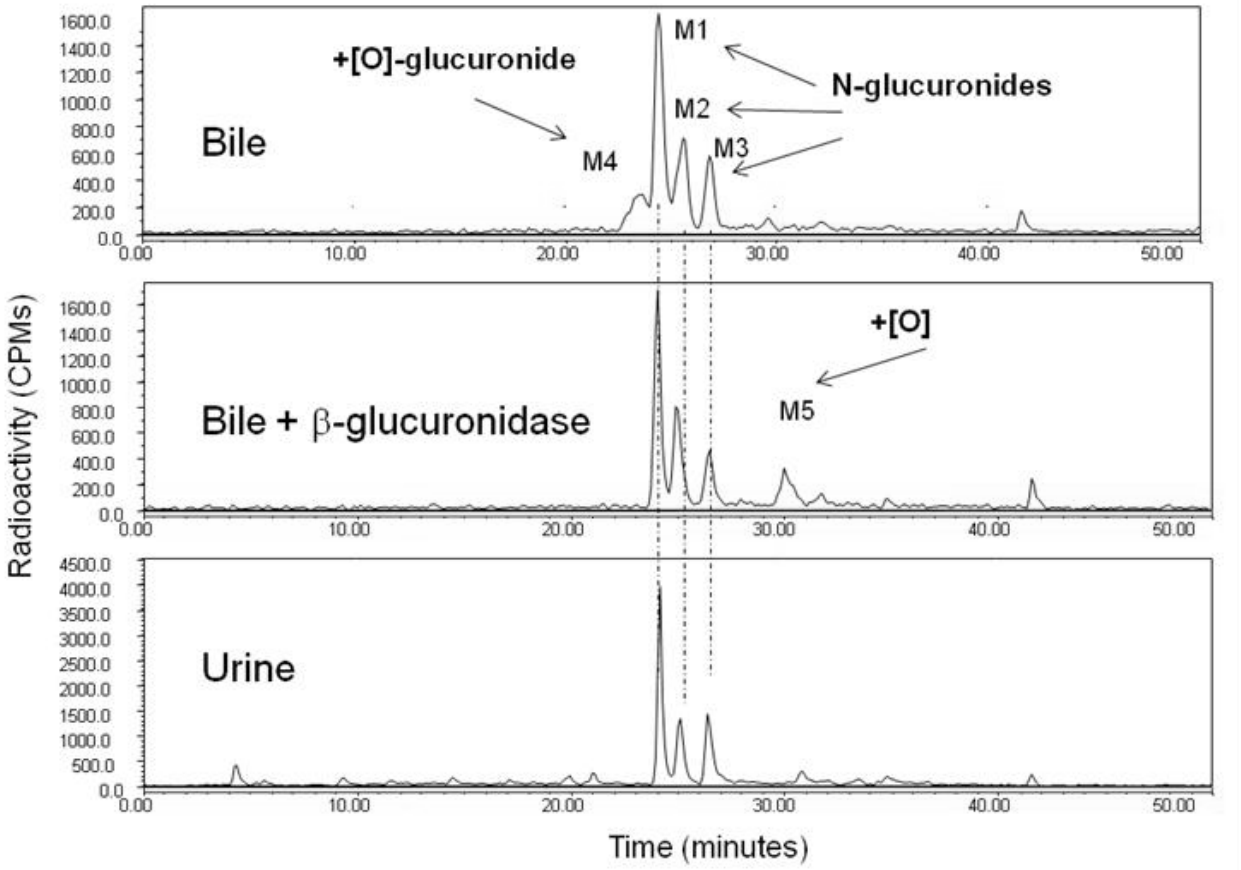

DMD Fast Forward. Published on January 14, 2014 as DOI: 10.1124/dmd.113.054809
This article has not been copyedited and formatted. The final version may differ from this version.

Figure 3

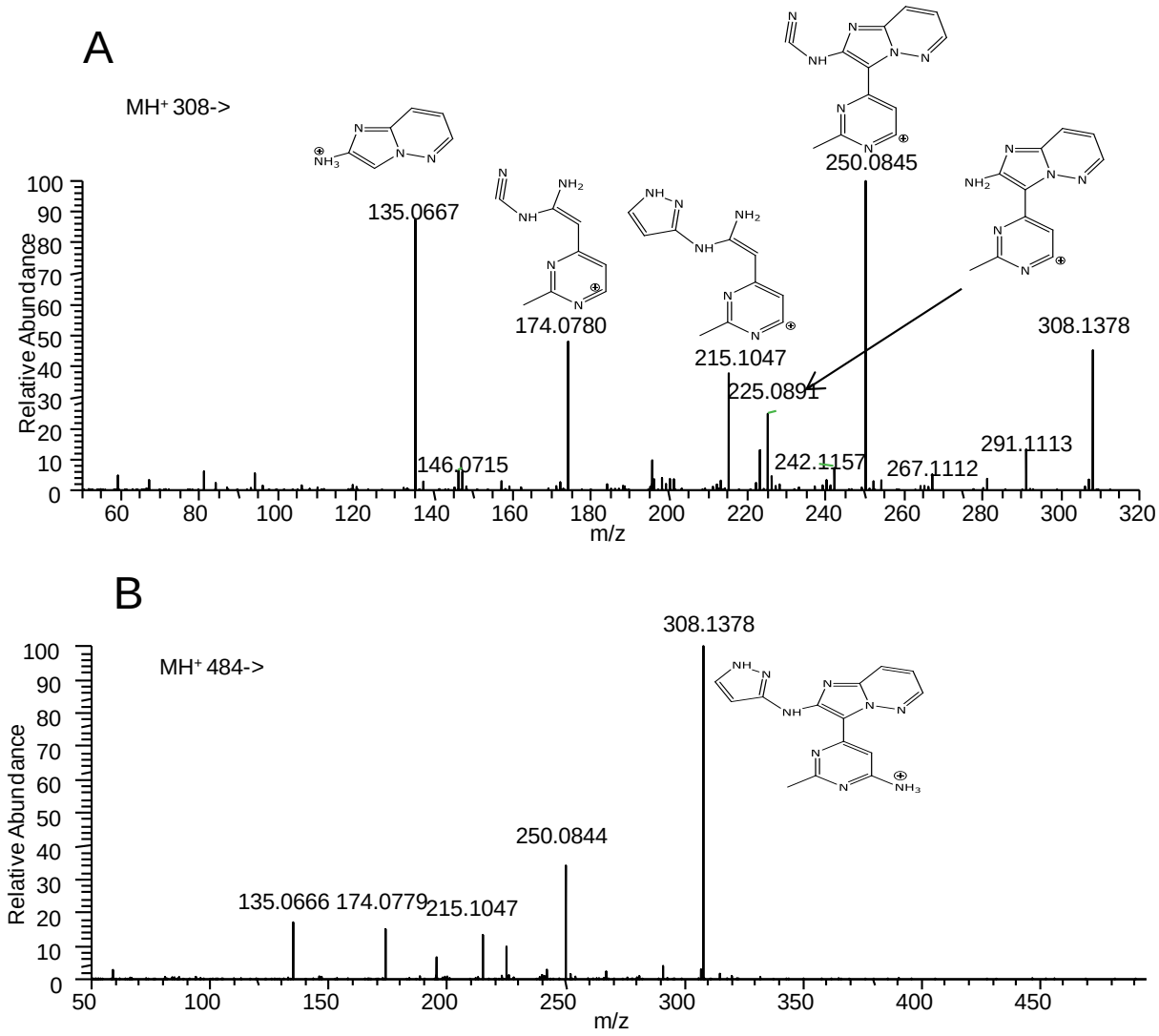

DMD Fast Forward. Published on January 14, 2014 as DOI: 10.1124/dmd.113.054809
This article has not been copyedited and formatted. The final version may differ from this version.

Figure 4

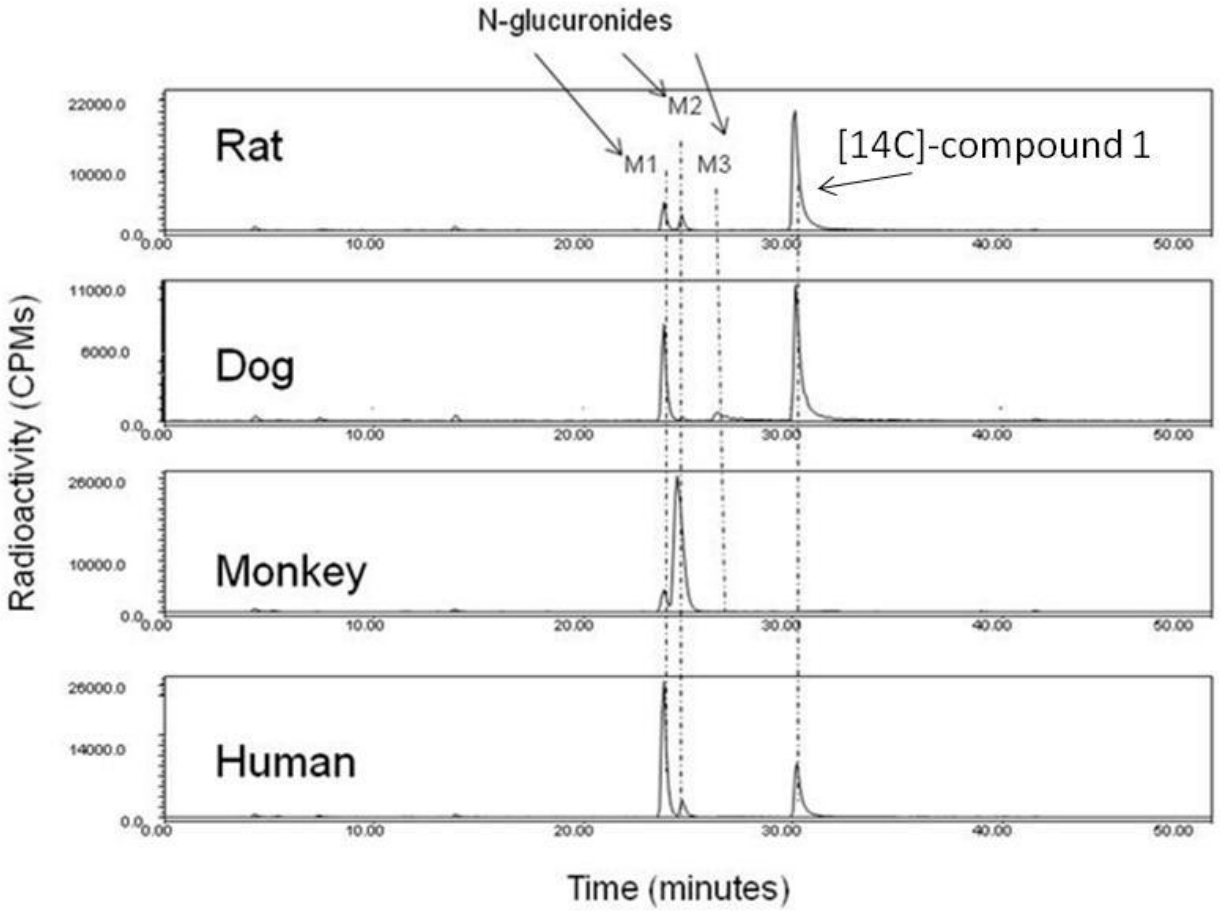

DMD Fast Forward. Published on January 14, 2014 as DOI: 10.1124/dmd.113.054809
This article has not been copyedited and formatted. The final version may differ from this version.

Figure 5

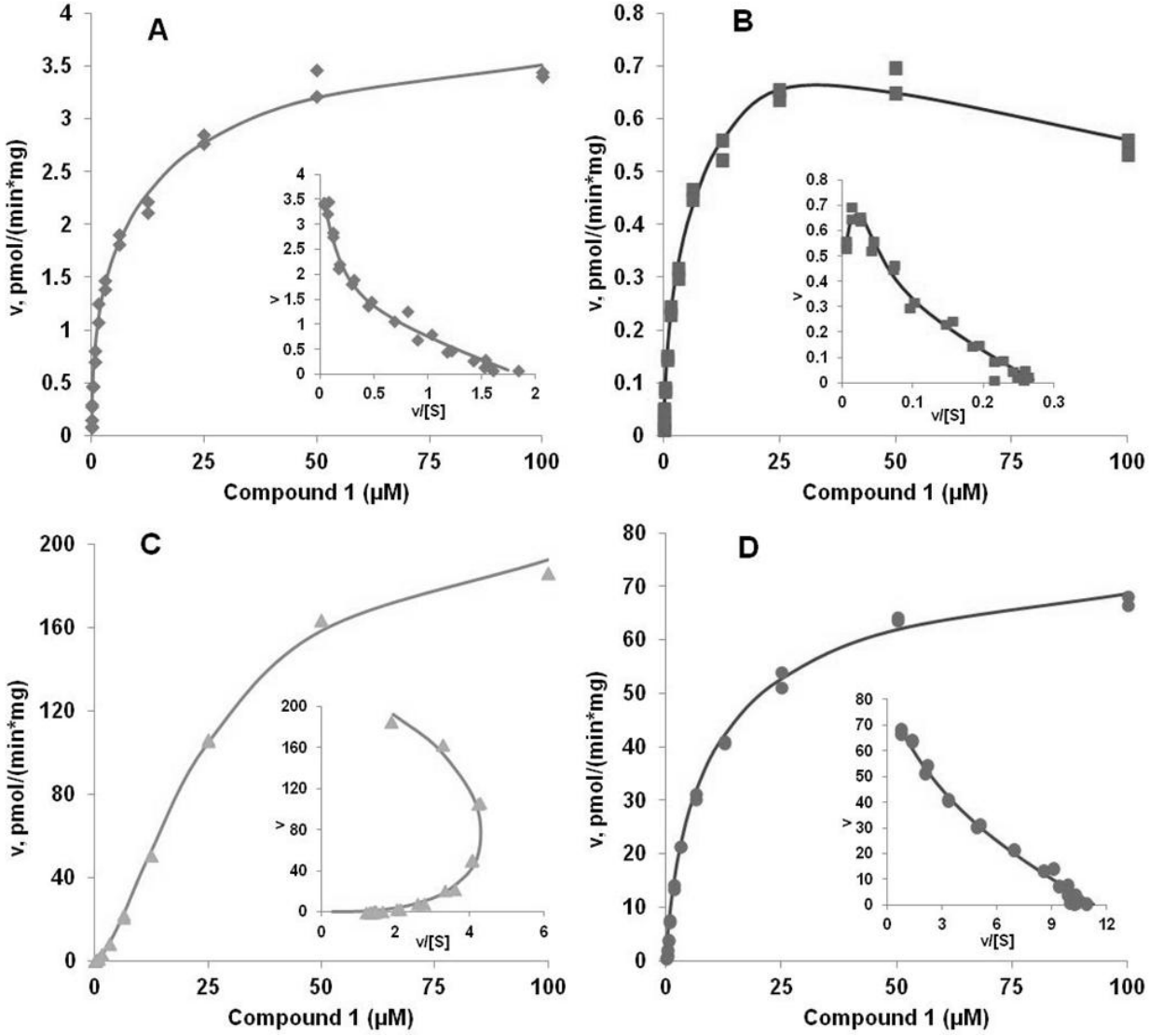

DMD Fast Forward. Published on January 14, 2014 as DOI: 10.1124/dmd.113.054809
This article has not been copyedited and formatted. The final version may differ from this version.

Figure 6

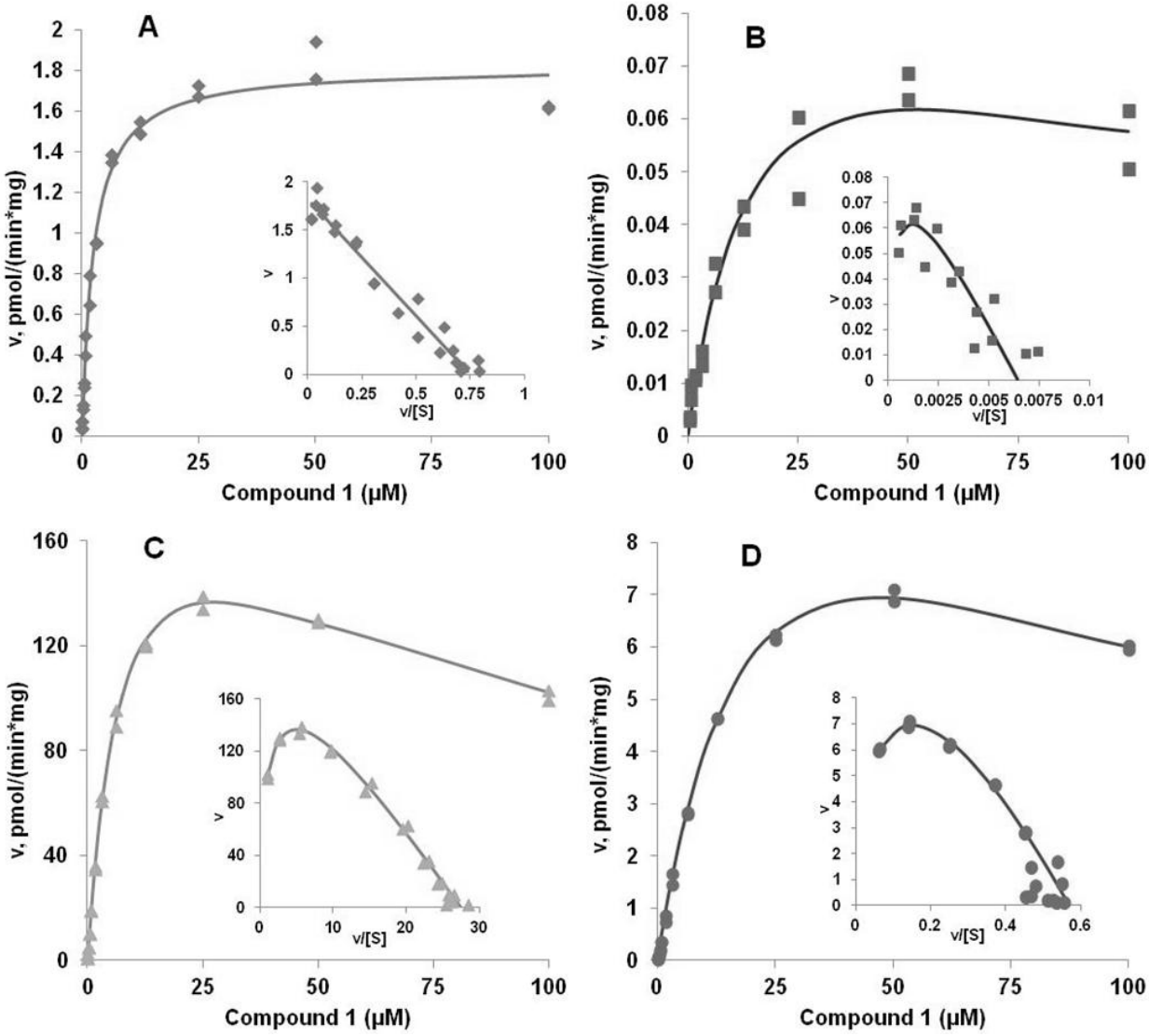

DMD Fast Forward. Published on January 14, 2014 as DOI: 10.1124/dmd.113.054809
This article has not been copyedited and formatted. The final version may differ from this version.

Figure 7

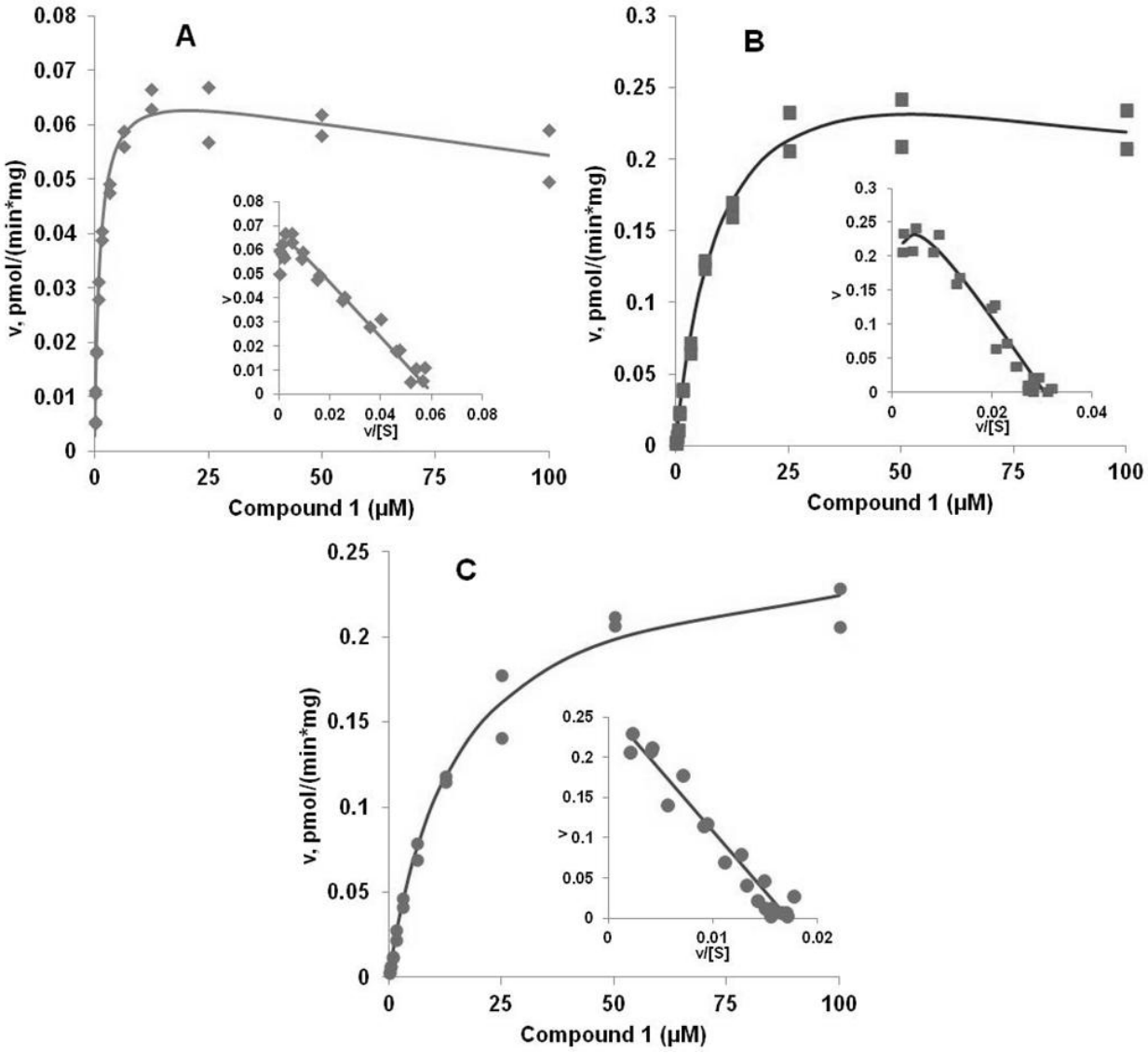

DMD Fast Forward. Published on January 14, 2014 as DOI: 10.1124/dmd.113.054809
This article has not been copyedited and formatted. The final version may differ from this version.

Figure 8